Rectangular Sandwich Plates with Miura-ori Folded Core under Quasi-Static Loadings

X.M. Xiang[a,b], Z. You[c], G. Lu[b*]

[a]*School of Civil Engineering, Guangzhou University, Guangzhou Panyu University City Outer Ring Road No. 230. Guangzhou 510006, China*

[b]*Faculty of Science, Engineering and Technology, Swinburne University of Technology, Hawthorn, Vic 3122, Australia*

[c] *Department of Engineering Science, University of Oxford, Parks Road, Oxford, OX1 3PJ, UK*

Abstract

This research presents a parametric study by using ABAQUS/Explicit and analytical analysis of rectangular sandwich plates with Miura-ori folded core. Two loading conditions are studied: three-point bending and uniformly distributed pressure loading. Load-displacement curves are obtained and energy absorption performance is assessed. Under three-point bending and uniformly distributed pressure loading of small magnitude, performance of such sandwich plates has been found to be better than that of corresponding monolithic plates of the same mass. In addition, analytical modelling has been conducted based on the plastic hinge theory, which results in a good agreement with those from the finite element analysis (FEA). It has been found that the maximum bending strength is governed by the incipience or fully plastic yielding of the core material for relatively thick cores, or elastic buckling of the core compression for thin cores. Furthermore, the yielding moment, fully plastic bending moment and elastic buckling moment of the incipience of core buckling have been evaluated.

Keywords: *sandwich plate; Miura-ori core; three-point bending; uniformly distributed pressure.*

* Corresponding author. Email: glu@swin.edu.au

1. Introduction

Sandwich structures are widely used in industries, such as aerospace, satellite, automotive, etc. due to their high energy absorption capacity and excellent bending strength with light weight. Different types of cores have been studied, including foam, truss, honeycomb and folded cores. Honeycombs are fully covered by the bonding faces of the sandwich panel, and hence water and vapours can get trapped inside the cells, which not only adds to the weight of the structure, but also increases the degradation of the mechanical performance. Discontinuous manufacturing process, vulnerability to impact loads and non-uniform failure mode during compressive loads are other disadvantages of honeycomb core [1]. Miura-ori, which is fabricated by folding the sheet along a pattern with straight and zigzag creases, may provide acoustic and heat insulation and act as energy absorbers [2]. Recently, 3D printing technology has been developed rapidly and it enables manufacturing of foldcores and trusses without imperfection [3]. The Miura origami pattern possesses some useful characteristics, such as developability, flat-foldability and rigid-foldability [4]. For military operation and disaster relief application, origami-inspired deployable shelters offer important advantages as they require a very small space in a folded form during transportation [5]. Compared with honeycomb core, air ventilation to avoid deterioration caused by long term moisture exposure is an additional advantage of foldcores.

Experimental and Finite Element Analysis (FEA) methods have been widely used to observe the mechanical behaviour of foldcores [6-9]. In the packaging and vehicle industries, sandwich structures are widely used as an energy absorber element and hence the energy absorption characteristic is an important performance. Recent studies on energy absorption of sandwich structures under quasi-static, low-velocity and high-velocity impact loads have revealed that a foldcore with high capacity is a suitable alternative for honeycomb cores [1, 7, 10-12]. Quasi-static, low velocity impact and high velocity impact on sandwich plates with foldcore were investigated experimentally and these experiments validated their corresponding modelling tests [13-15]. It is evident that FEA is suitable for the development of core geometries for specific requirements. FEA can not only be used for the complete

characterisation of the mechanical behaviour under compression, tension or shear loading in both in-plane and out-of-plane directions, but also allows for a detailed investigation of cell wall deformation patterns and failure modes, which are otherwise difficult to observe through experiment [16]. Quasi-static compression and blast loading on sandwich plate with Miura-ori foldcore were investigated by means of FEA and a parametric study was conducted by altering the fold pattern [17]. It has been found that the compressive collapse strength of the stacked folded core is comparable to other bending dominated cellular materials, such as foams and honeycombs [17].

Large deformation of metal sandwich structures with foldcore under three-point bending and static pressure loadings has not been investigated so far. Besides, an analytical study of this topic has not been presented. In this paper, a parametric study of sandwich plates with Miura-ori foldcore is first investigated. Quasi-static three-point bending and uniformly distributed pressure loading are investigated. The maximum bending strength and energy absorption are compared for sandwich plates with different parameters. The yielding moment, fully plastic bending moment and elastic buckling moment of the incipience of core buckling are analysed. The load capacity and energy absorption capacity of the sandwich plates are compared with those of the corresponding monolithic plates of the same mass.

2. Geometry of Miura-ori core

2.1 Parameters of a Miura-ori core

Miura-ori is fabricated by folding a sheet along a pattern with straight and zigzag creases. The unfolded unit cell consists of four identical parallelograms defined by four parameters, i.e., side lengths a, b and sector angle ϕ (Fig. 1(a)). Fig. 2 demonstrates the folding state of the Miura-ori pattern. This folding progress introduces four other parameters: two lateral dihedral angles θ_A and θ_Z; two edge angles η_A and η_Z (see Fig. 1 (b)). m and n are the number of units in width and longitudinal directions (shown in Fig. 2), respectively.

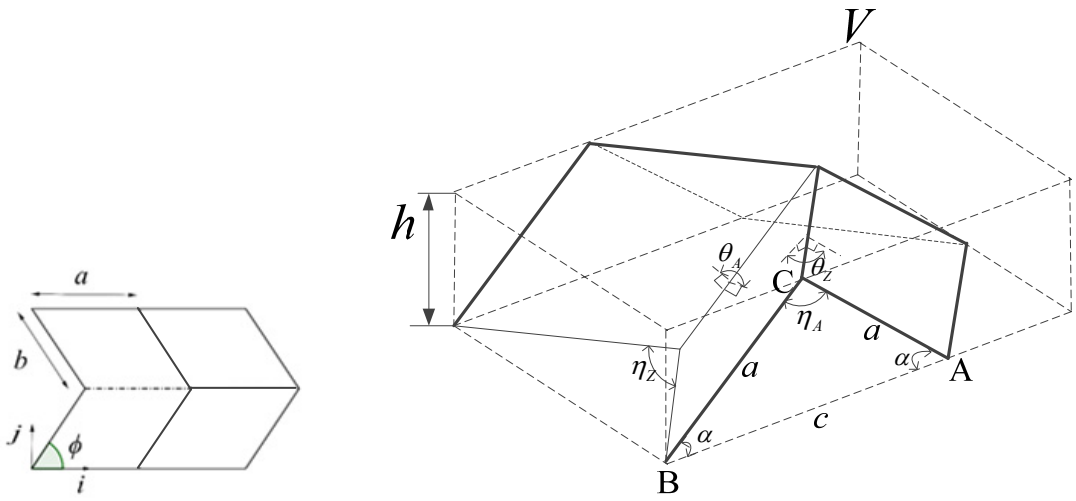

(a) (b)

Fig. 1 Parameters of a Miura-ori core: (a) an unfolded Miura-ori unit cell; (b) dihedral and edge angles of a folded unit cell

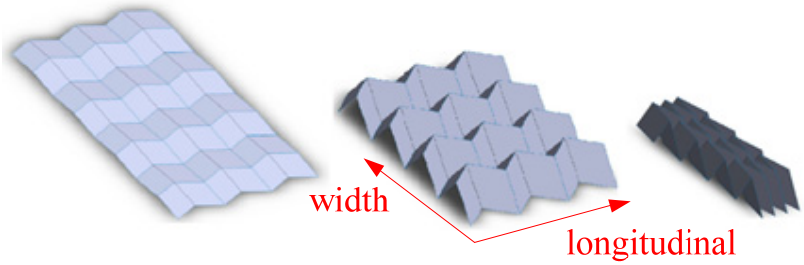

Fig. 2 Folding states of a Miura-ori core

2.2 Nominal density of a folded unit

Side lengths (a and b), sector angle (ϕ) and lateral dihedral angle (θ_A) (see Fig. 1) are defined as the input values, and the other parameters can be calculated by the following equations [10].

The lateral dihedral angles θ_Z is

$$\theta_Z = \arccos\left[\frac{(\cos\theta_A - 1)(\cos 2\phi - 1) + 4\cos\theta_A}{4 - (\cos\theta_A - 1)(\cos 2\phi - 1)}\right] \tag{1}$$

The edge angle η_Z is

$$\eta_Z = \arccos(\sin^2\phi\cos\theta_A + \cos^2\phi) \tag{2}$$

The edge angle η_A is

$$\eta_A = \arccos(\sin^2\phi\cos\theta_Z - \cos^2\phi) \tag{3}$$

The height of the unit cell (shown in Fig. 1(b)) is

$$h = a\cos\frac{\eta_A}{2} \tag{4}$$

The surface area of each unit cell is

$$S = 4ab\sin\phi \tag{5}$$

The volume occupied by each unit of a rectangular circumscribing block (shown in Fig. 1(b)) is

$$V = 2bh\sin\frac{\eta_Z}{2}(2a\sin\frac{\eta_A}{2} + b\cos\frac{\eta_Z}{2}) \tag{6}$$

and the volume of solid is St, where t is the thickness of the base material sheet .

The nominal density of the Miura-ori is given by

$$\rho = \frac{\rho_m St}{V} \tag{7}$$

where ρ_m is the density of the base material.

The relative density is

$$\frac{\rho}{\rho_m} = \frac{St}{V} = \frac{4t\sin\phi}{2a\sin\eta_A\sin\frac{\eta_Z}{2} + b\cos\frac{\eta_A}{2}\sin\eta_Z} \tag{8}$$

Variation of the relative density of a Miura-ori core against θ_A and ϕ are shown in Fig. 3, where a=b=35 mm, t=0.6 mm and $\rho_m = 7800\,kg/m^3$. For the ϕ- density curve, θ_A is 83^0, while for the θ_A- density curve, ϕ is set as 66^0.

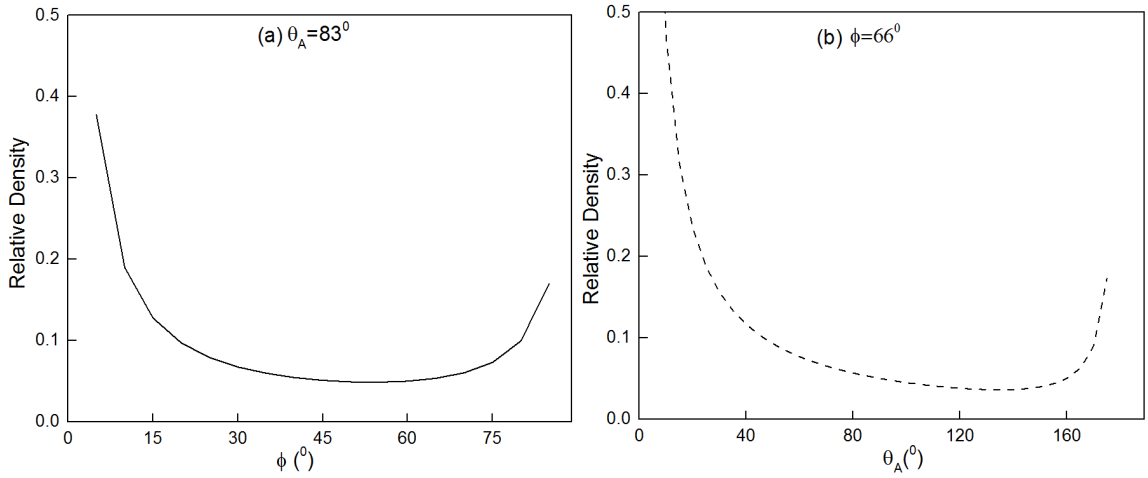

Fig. 3 Relative density of a Miura-ori core: (a) Density-ϕ and (b) Density-θ_A

3. Finite Element Analysis (FEA)

3.1 Sandwich panel models for FEA

Several cases of sandwich panels were analysed with two loading conditions: quasi-static three-point bending and uniformly distributed pressure loading (see Fig. 4). The core models were developed using SolidWorks. FEA was conducted by using ABAQUS/Explicit. The core and the face plate were tied together. The elements of the models were linear quad shell element, type S4R and the mesh size was 2 *mm*. The material was a typical mild steel without strain hardening and its density is 7800 kg/m^3, Young's modulus is 210 *GPa* and yield stress is 200 *MPa*.

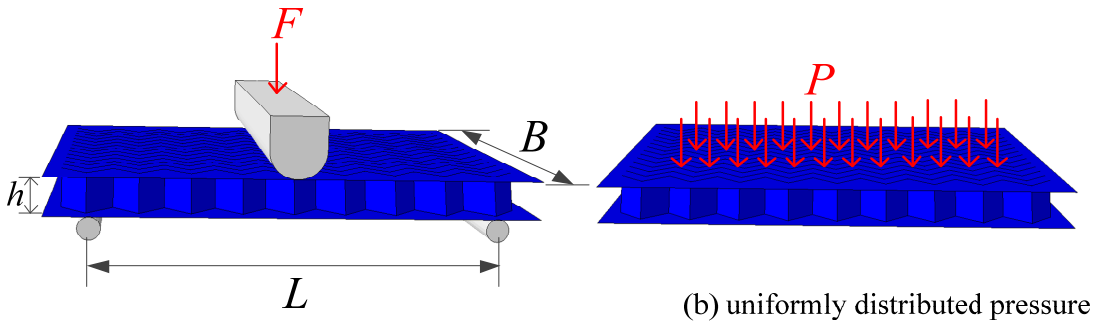

(a) three-point bending

(b) uniformly distributed pressure loading

Fig. 4 Two loading conditions

The area of the face sheet was 430 *mm* by 400 *mm* (width of the plate, *B*, see Fig. 4(a)). The thickness of all the face sheet was 5 *mm* and the mass of each face sheet was 6.71 *kg*. *m* and *n* were adjusted to make the overall dimensions of the Miura-ori cores as 430 *mm* by 400 *mm*. For the core, ϕ, θ_A and side lengths (*a* and *b*) were set as variables of the Miura-ori core, but their values were such that the total mass remained the same. Each core had the same mass, 2.09 *kg*, and the thickness of the core (*t*) was different.

Panels with three groups of cores were generated and studied in order to investigate the effect of various parameters. The top and bottom skins were the same. Group 1 had cores with different values of sector angles, ϕ, while *t* was adjusted accordingly to keep the mass constant. Group 2 was for cores with different lateral dihedral angles, θ_A, while Group 3 had cores with different side lengths, *a* and *b*.

3.1.1 Cores with different values of sector angle, ϕ (Group 1)

The lateral dihedral angle and side lengths were fixed at constant values ($\theta_A = 83^0$ and *a*=*b*=35 *mm*) and ϕ was chosen as five different values: 45^0, 55^0, 66^0, 75^0 and 80^0, respectively. All the Miura-ori core models had the same mass. The core models, thickness of the shell elements, height of the core, and number of cells on each side when $\phi = 45^0$ and 80^0 are shown in Fig. 5. respectively. As the value of ϕ increases the model becomes more compact in the width (y) direction. Also, thickness of the shell elements decreases and the height increases.

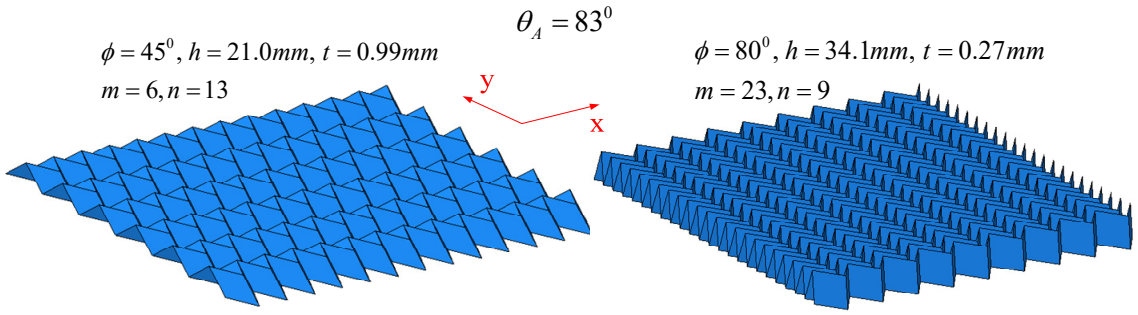

Fig. 5 Miura-ori cores with different sector angles, ϕ (Group 1, $\theta_A = 83^0$ and a=b=35 mm)

3.1.2 Cores with different values of lateral dihedral angle, θ_A (Group 2)

In this group, the sector angle and side lengths were fixed at constant values ($\phi = 66^0$ and a=b=35 mm) and θ_A was chosen as five different values: 45^0, 60^0, 75^0, 95^0 and 135^0, respectively. Again, all the Miura-ori core models had the same mass. For $\theta_A = 45^0$ and 135^0, respectively, the core models with the information of the thickness, height and number of cells on each side are also shown in Fig. 6. It can be seen that the model becomes less compact in both the longitudinal (x) and width (y) directions as θ_A increases. When the value of θ_A increases, the thickness of the shell elements increases while the height of the core decreases slightly.

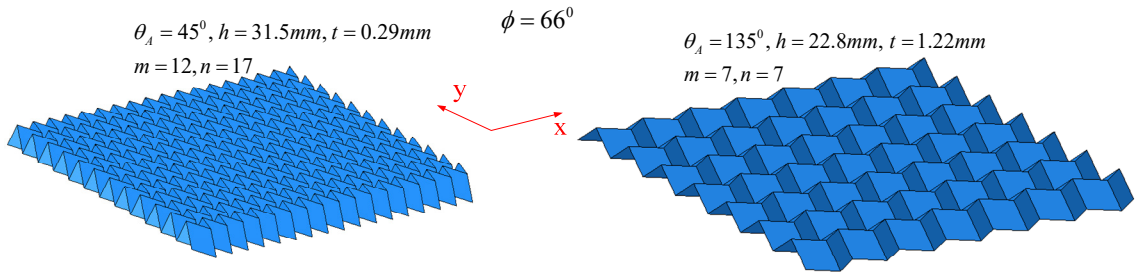

Fig. 6 Miura-ori cores with different lateral dihedral angles, θ_A (Group 2, $\phi = 66^0$ and a=b=35 mm)

3.1.3 Cores with different values of side lengths, *a* and *b* (Group 3)

Both the sector angle and lateral dihedral angle were fixed at constant values ($\phi = 66^0$ and $\theta_A = 83^0$) and side lengths were chosen as four different groups: *a*=*b*=25 *mm*, *a*=*b*=35 *mm*, *a*=*b*=50 *mm*, *a*=67 *mm* and *b*=70 *mm*, respectively. The core models with different side lengths are shown in Fig. 7. The number of cells on each side decreases with the increasing side length proportionally. The model becomes less compact in both the x and y directions with the increasing side length. Thickness of the shell elements is the same for different cores, while the height increases with the increasing side length linearly.

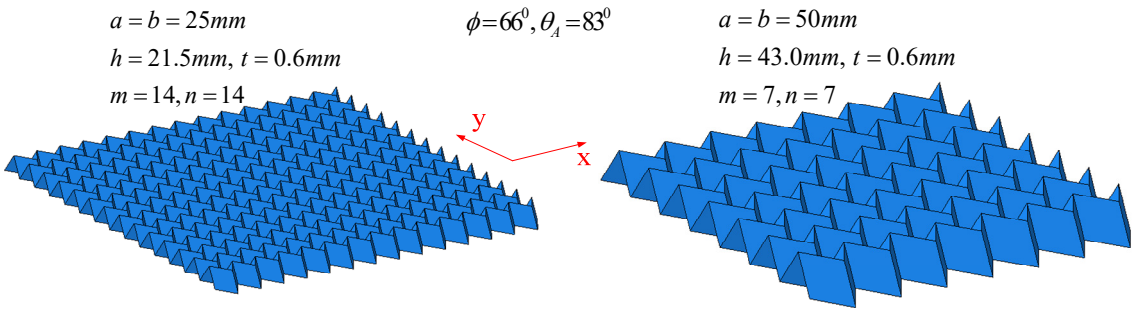

Fig. 7 Miura-ori cores with different side lengths (Group 3, $\phi = 66^0$ and $\theta_A = 83^0$)

3.2 Sandwich panel under three-point bending

Response of a sandwich plate with Miura-ori core under three-point bending load is studied (see Fig. 8, where *d* is the displacement of the indenter and the plot contours denote the von Mises stress). In the FE model, the indenter and the supports were set as rigid body and the value of friction coefficient was 0.01 for all the contacts. The diameter of the semicircular indenter head was 50 *mm*. The indenter and the supports were along y direction and the distance of the support span (*L,* see Fig. 4(a)) was 352.6 *mm*. Three loading rates, i.e. 0.04 m/s, 0.1 m/s and 0.4 m/s, were applied, respectively. The force-displacement curves are shown in

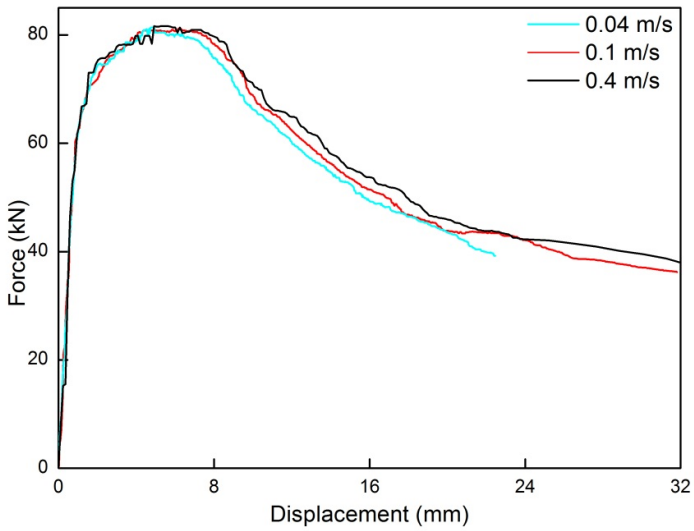

Fig. 9 and the three curves are almost identical. The maximum discrepancy in the peak force was within 5% and, therefore, velocity of 0.4 m/s was chosen in this work.

For the case of $\phi = 55^0$ and $\theta_A = 83^0$, the displacement at the mid-span of the top and bottom face sheets is plotted in Fig. 10. The horizontal axis is the displacement of the indenter and the vertical axis is the displacement at the mid-span of the two face sheets. The displacement at the mid-span of the bottom face sheet is less than that at the top face (also the indenter displacement). The difference between them indicates the compression of the core. It shows that at the early deformation stage, the sandwich plate deforms as a whole with little core compression, and then the core becomes increasingly compressed. The relationship between the force and displacement of the indenter is shown in Fig. 11. The force increases almost linearly and then it reaches a peak ($F_{\max}$). Fig. 8 (b) shows the deformation of the sandwich plate when $F = F_{\max}$. Subsequently, the force decreases when the displacement increases, indicating a softening behavior. It appears that localized deformation occurs around the central region of the panel (see Fig. 8 (c) and (d)) and the local indentation of the top face sheet occurs at the late stage of the deformation (see Fig. 8 (d)).

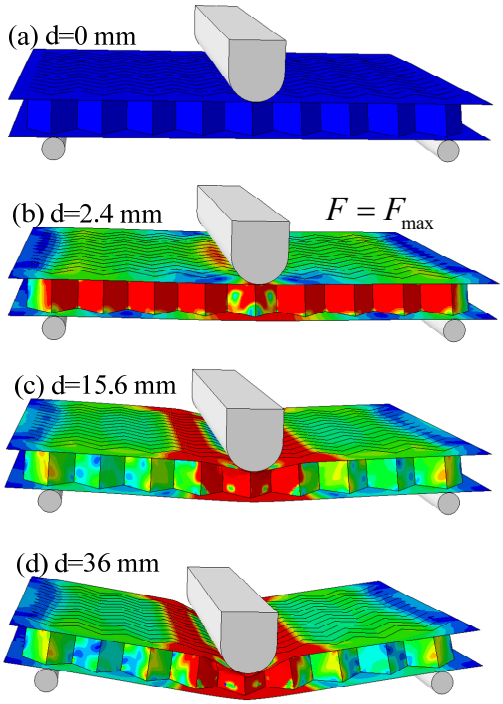

Fig. 8 Deformed shape of a sandwich panel ($\phi = 75^0$ and $\theta_A = 83^0$) under three-point bending: (a) *d*=0 *mm*; (b) *d*=2.4 *mm*; (c) *d*=15.6 *mm*; (d) *d*=36 *mm*

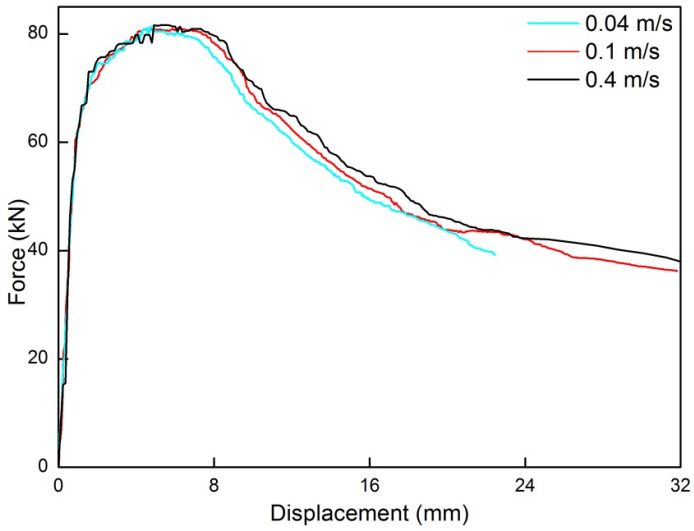

Fig. 9 Force-displacement curves for a sandwich panel under three different loading rates

Plastic energy absorption corresponding to an indenter displacement of 30 *mm* was exported from ABAQUS software (see Fig. 12). It can be seen that when $\phi = 55^0$ and $\phi = 66^0$, sandwich plates have the best energy absorption capacity (see Fig. 12(a)), and the one with

$\phi = 55^0$ has slightly lower peak force and longer plateau of the compressive force (see Fig. 11(a)). In Fig. 11(a) when $\phi = 75^0$, the sandwich plate achieves the highest peak force, but undergoes subsequent significant softening due to buckling within the core. The values of the peak force ($F_{\max}$) and energy absorption are listed in Table 1 and it is found that in Group 1 the maximum difference of $F_{\max}$ is 15%. From Fig. 11(b) and Fig. 12(b), the sandwich plate with $\theta_A = 95^0$ has the best energy absorption and the highest peak force. In Group 2 the maximum difference of $F_{\max}$ is 40%. From Fig. 11(c), for different side lengths, peak force is almost the same except for the one with side length *a*=67 *mm* and *b*=70 *mm* and the maximum difference of $F_{\max}$ is 9% in Group 3. Softening due to core buckling is prone to taking place as the side lengths increase. Energy absorption capacity decreases as the side lengths increase (see Fig. 12(c)).

Three-point bending on a corresponding monolithic plate with the same mass and size was also analyzed. The thickness of the monolithic plate was 11.6 *mm*. Force-displacement relationship and plastic energy absorption are also shown in Fig. 11 and Fig. 12. A comparison of the two structures under three-point bending load will be made in Section 5.

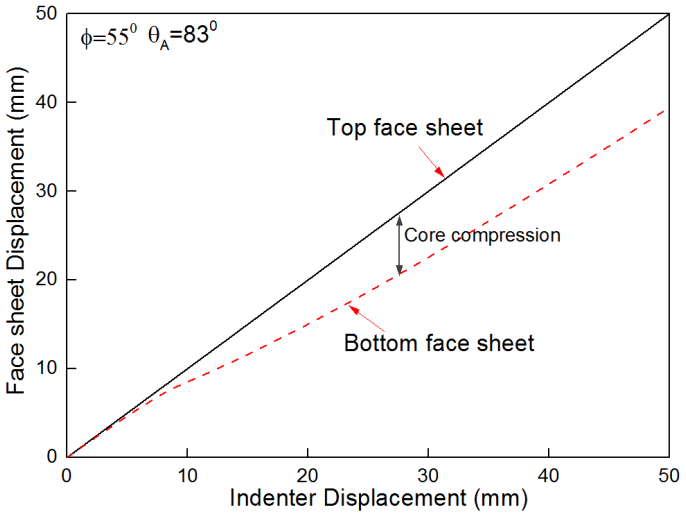

Fig. 10 Displacement at the mid-span of the top and bottom face sheets for the specimen with $\phi = 55^0$ and $\theta_A = 83^0$

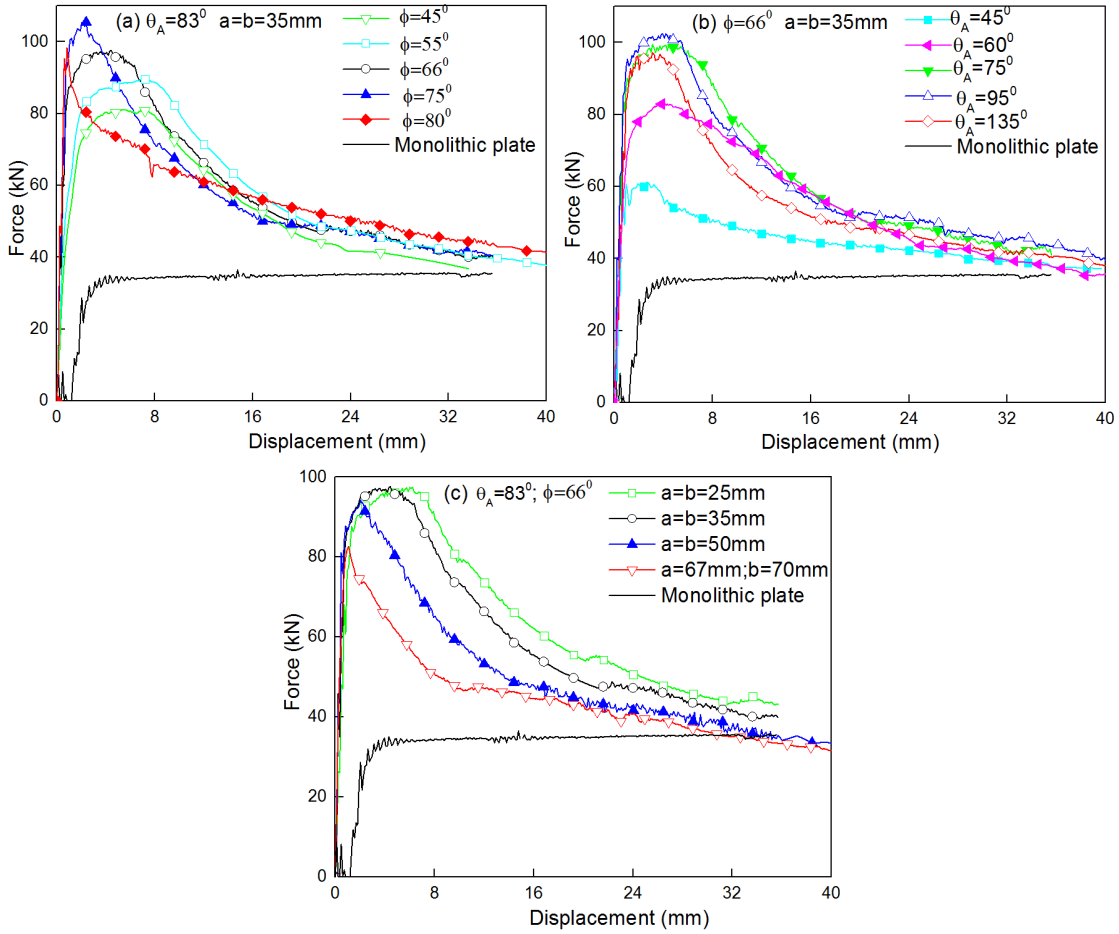

Fig. 11 Force-displacement curves under quasi-static three-point bending: (a) different values of ϕ; (b) different values of θ_A; (c) different values of side lengths

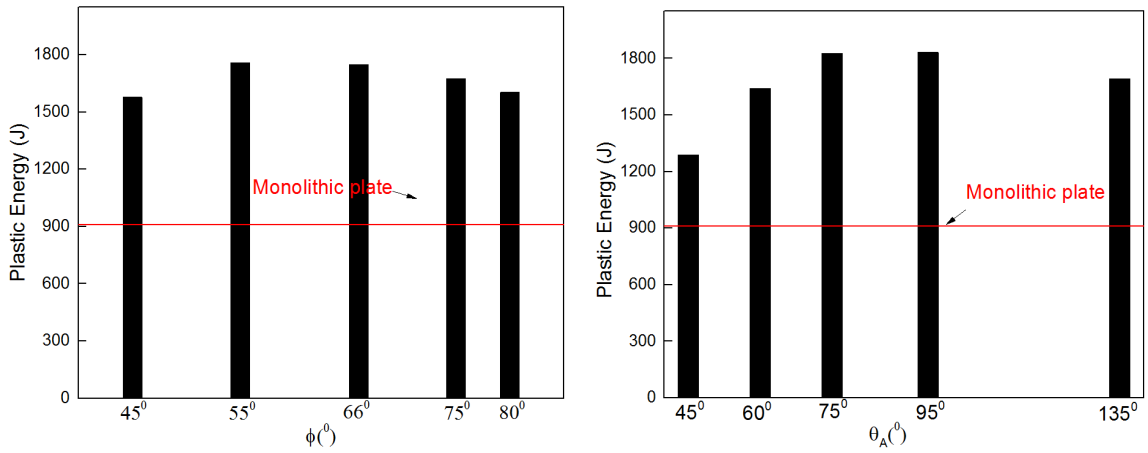

(a) $\theta_A = 83^0$, a=b=35 mm (b) $\phi = 66^0$, a=b=35 mm

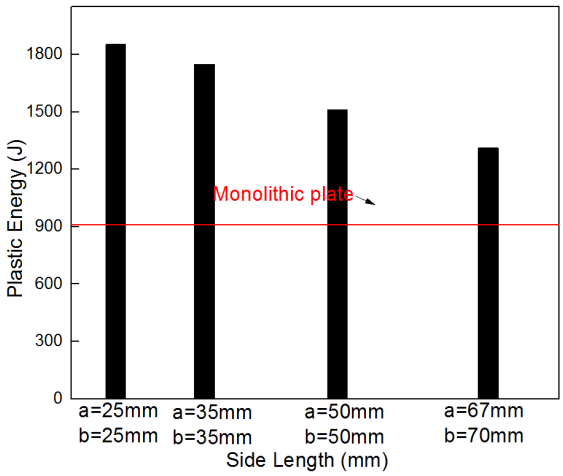

(c) $\phi = 66^0$, $\theta_A = 83^0$

Fig. 12 Plastic energy under quasi-static three-point bending: (a) different values of ϕ; (b) different values of θ_A; (c) different values of side lengths

Table 1 Results from FEA and theoretical analysis

Group No.	a (mm)	b (mm)	ϕ (^{0})	θ_A (^{0})	t (mm)	$F_{\max}(FEA)$ (kN)	$Energy(FEA)$ (J)	$M_{\max}$ ($kN*m$)	σ_b (MPa)
	35	35	45	83	0.994	90.0	1578	7.9	187.2
	35	35	55	83	0.869	94.7	1759	8.3	161.5
1	35	35	66	83	0.600	97.6	1749	8.6	141.6
	35	35	75	83	0.450	105.5	1676	9.3	139.5
	35	35	80	83	0.269	98.3	1604	8.7	125.8
	35	35	66	45	0.294	61.2	1287	5.4	85.9
	35	35	66	60	0.420	85.3	1641	7.5	120.6
2	35	35	66	75	0.600	99.5	1826	8.8	142.3
	35	35	66	95	0.741	102.4	1832	9.0	152.3
	35	35	66	135	1.224	99.6	1692	8.7	187.8
	25	25	66	83	0.6	97.4	1853	8.6	197.8
3	35	35	66	83	0.6	97.6	1749	8.6	141.6
	50	50	66	83	0.6	94.1	1513	8.3	95.5
	67	70	66	83	0.627	88.5	1312	7.8	65.6

3.3 Sandwich panel under uniformly distributed pressure

Response of the previous sandwich plates with Miura-ori core but under uniformly distributed pressure is studied (see Fig. 13). The four edges of the sandwich plates were clamped and the

area exposed to pressure was 352.6 *mm* by 328 *mm*. The applied pressure was from 3 *MPa* to 7 *MPa*.

When $\phi = 66^0$ and $\theta_A = 135^0$, the displacement at the middle of the top and bottom face sheets is plotted in Fig. 14. The horizontal axis is the pressure and the vertical axis is the displacement at the middle of the two face sheets. The difference between the two curves indicates the compression of the core. It shows that when pressure is small, the sandwich plate deforms as a whole, and the core compression increases with the increasing pressure. Displacement at the middle of the bottom plate at different amplitudes of pressure loading is shown in Fig. 15. When pressure is large, some data in Fig. 15(c) were missing due to the severely distorted elements near the clamp boundary. The core compression at the middle of the plates is plotted in Fig. 16, which shows that the core compression increases with the increasing sector angle ϕ and side length (see Fig. 16(a) and (c)). When the side length is small, the core has no compression even when pressure is large (see Fig. 16(c)).

Total plastic energy absorption is shown in Fig. 17 and it has the same trend as for the core compression. It is because the plastic energy absorbed by the core is more than half of the total plastic energy, while the face sheets absorb almost the same amount of plastic energy for all the different sandwich plates. When the final displacement is small, i.e. less than 40 *mm*, the plastic energy absorption has almost the same value for models with different sector and dihedral angles. When the final deformation is large, the plastic energy absorption increases as sector angle increases. However, as the dihedral angle increases it firstly decreases until θ_A is around 75^0 and then increases. The plastic energy absorption increases with the increasing of side length, especially when the deformation is large.

Corresponding monolithic plate loaded with uniformly distributed pressure was also studied, which had the same mass and overall dimensions for the sandwich plates. Force-displacement relationship and plastic energy absorption are also shown in Fig. 15 and Fig. 17 respectively. A comparison of the two structures will also be made in Section 5.

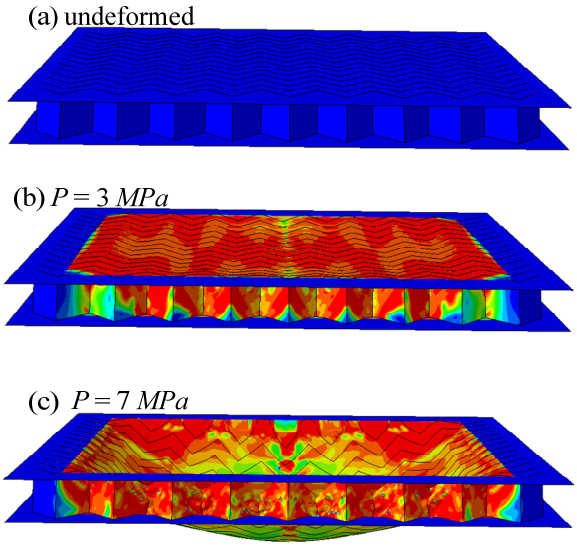

Fig. 13 Deformed shape of a sandwich panel ($\phi = 75^0$ and $\theta_A = 83^0$) under uniformly distributed pressure: (a) undeformed; (b) P=3 *MPa*; (c) P=7 *MPa* (the plot contours denote the Mises Stress)

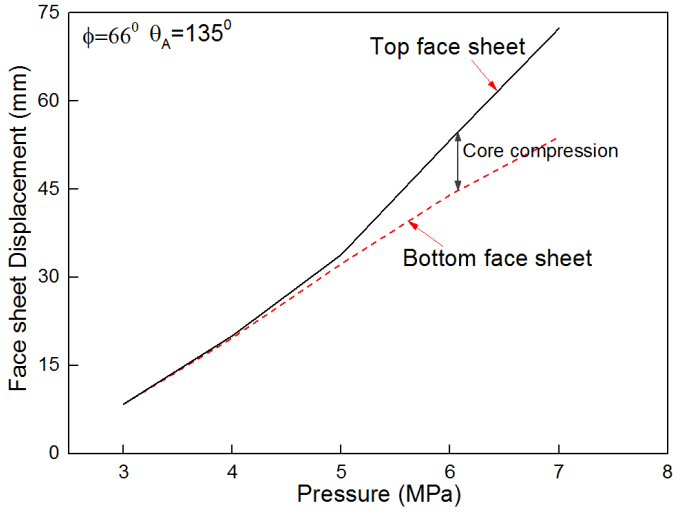

Fig. 14 Displacement at the middle of the top and bottom face sheets ($\phi = 66^0$, $\theta_A = 135^0$ and a=b=35mm)

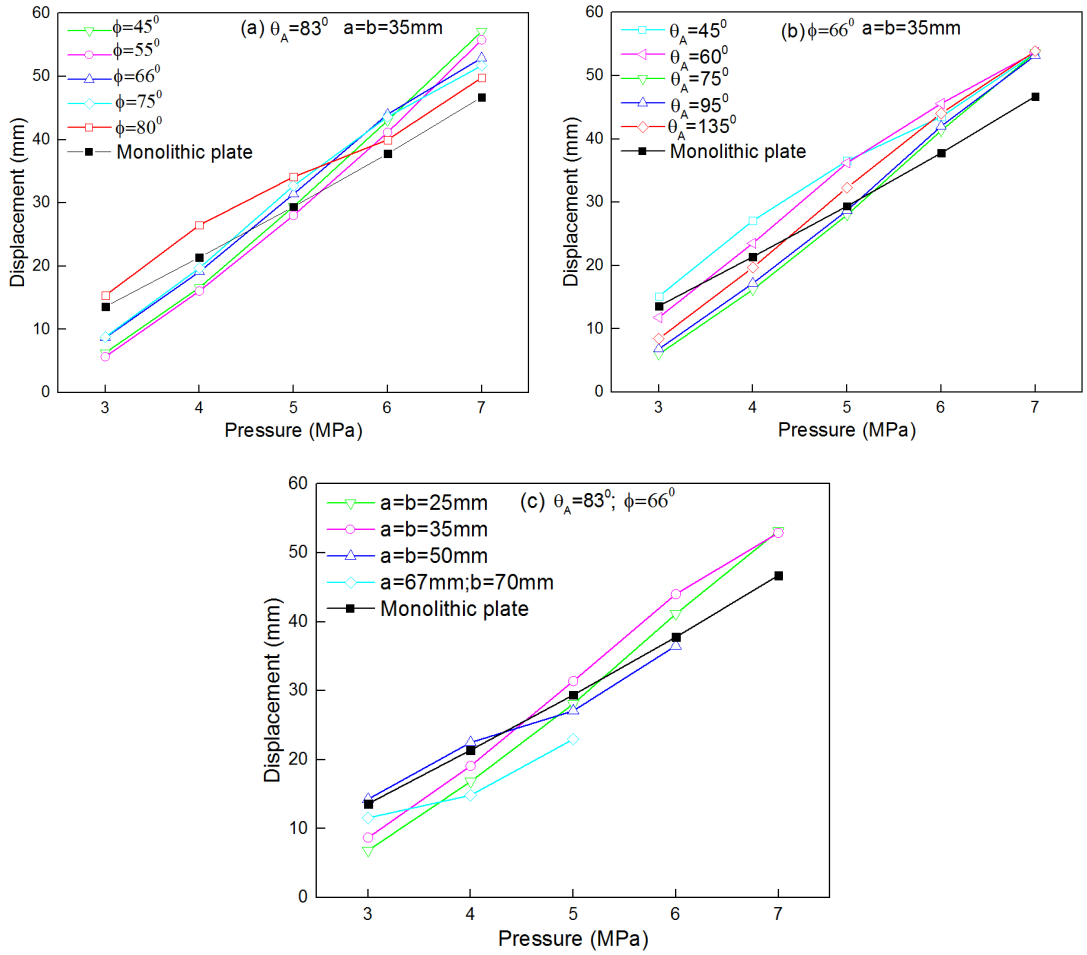

Fig. 15 Displacement-pressure curves under uniformly distributed pressure: (a) different values of ϕ; (b) different values of θ_A; (c) different values of side lengths

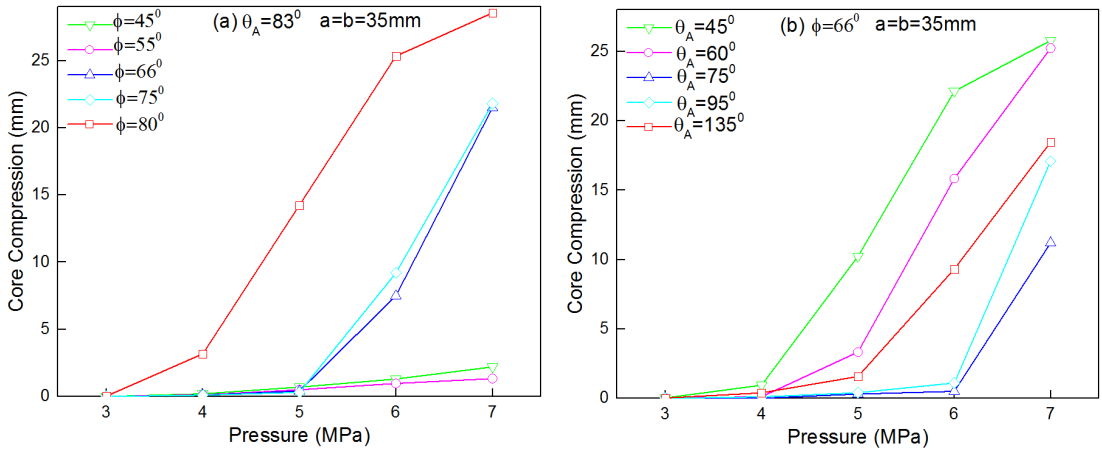

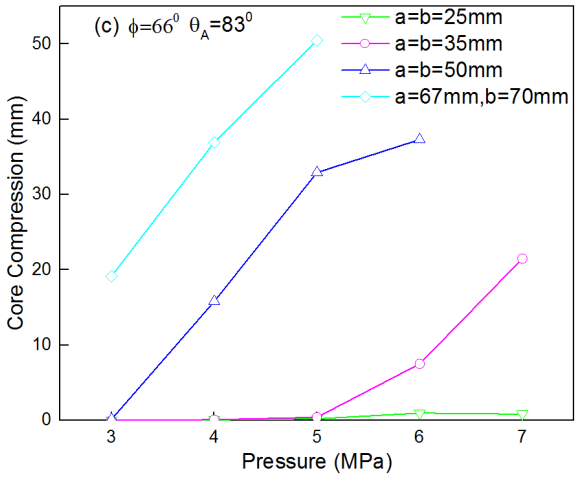

Fig. 16 Core compression under uniformly distributed pressure: (a) different values of ϕ; (b) different values of θ_A; (c) different values of side lengths

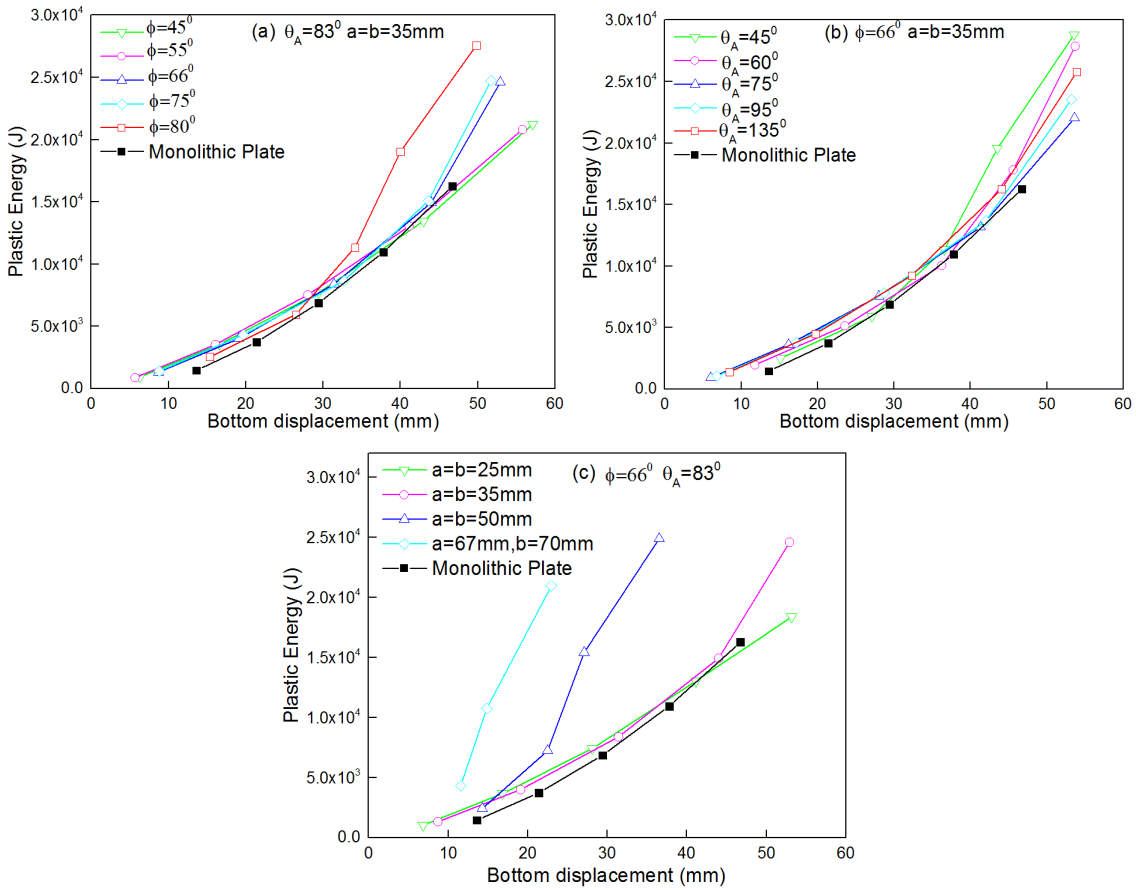

Fig. 17 Plastic energy under uniformly distributed pressure: (a) different values of ϕ; (b)

different values of θ_A; (c) different values of side lengths

4. Analytical consideration of sandwich plates

The maximum bending strength is governed by the incipience or fully plastic yielding of the core material for relatively thick cores, or elastic buckling of the core compression for thin cores. The incipience of yielding moment (M_Y), fully plastic bending moment (M_p) and elastic buckling moment (M_b) of the incipience of core buckling will be discussed in this section.

4.1 Yielding moment, M_Y

Fig. 18 (a) shows the cross-section of a Miura-ori core along the width direction at an arbitrary position. A sketch of cross-section of the sandwich plate with a width of one unit cell is plotted in Fig. 18 (b) and the cross-section of one Miura-ori core cell unit (ΔABC) is also shown in Fig. 1 (b). The neutral axial is located at the middle of the height. Under the bending load, the stress above the neutral axis is compressive and the stress below it is tensile. Fig. 18 (c) shows the stress distribution on the cross-section of the sandwich plate when the material at the top and bottom of the core starts to yield. Since the thickness of the face sheet is much thinner than the height of the core, it is assumed that the stress on the cross-section of the face sheet is uniformly distributed through the face sheet thickness. The expression of the yielding moment is

$$M_Y = \frac{\sigma_Y \cdot I_y}{h/2} \tag{9}$$

where σ_Y is the yield stress of the material and I_y is the cross-sectional moment of inertia of the y axis, which is

$$\begin{aligned} I_y &= 2m\int_0^{\frac{h}{2}} \frac{2t}{\sin\alpha} z^2 dz + 2Bt_f\left(\frac{h}{2}\right)^2 \\ &= \frac{mth^3}{6\sin\alpha} + \frac{Bt_f h^2}{2} \end{aligned} \tag{10}$$

where t is the thickness of the core material, m is the number of cells in the y direction, B and t_f is the width and thickness of the face sheet. In the triangle ABC in Fig. 18 (b), $\frac{a}{\sin\alpha}=\frac{c}{\sin\eta_A}$ and $a^2\sin\eta_A=ch$. Therefore, the yielding moment can be derived from Eqs.(9) and (10),

$$M_Y=\sigma_Y\left(\frac{mth^2}{3\sin\alpha}+Bt_fh\right) \tag{11}$$

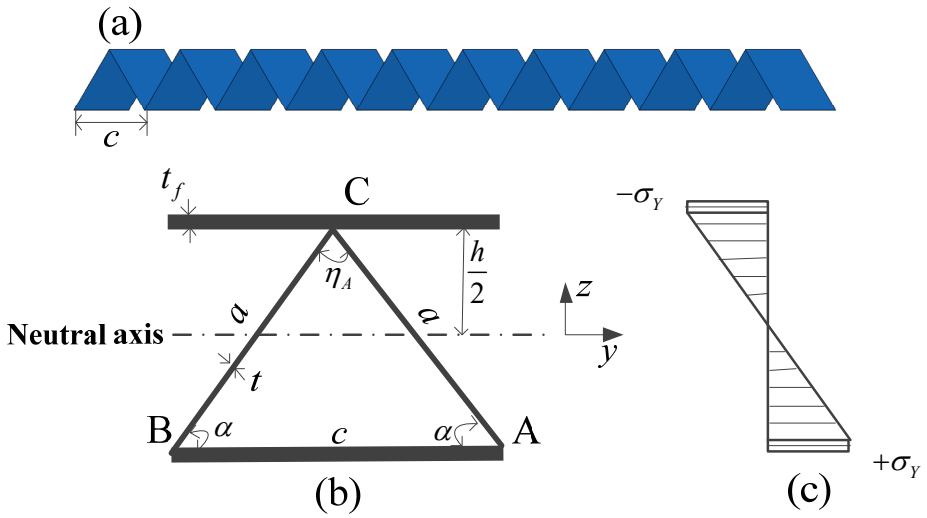

Fig. 18 Yielding moment: (a) cross-section of the core; (b) sketch of cross-section of the sandwich plate with a width of one unit cell; (c) stress distribution

4.2 Fully plastic bending moment, M_p

When the material at the cross-section is at the fully plastic state, the stress distribution is shown in Fig. 19(b). The fully plastic bending moment at the cross-section is

$$\begin{aligned}M_p&=2m\sigma_Y\int_0^{\frac{h}{2}}\frac{2t}{\sin\alpha}zdz+\sigma_YBt_fh\\&=\frac{m\sigma_Yth^2}{2\sin\alpha}+\sigma_YBt_fh\end{aligned} \tag{12}$$

$M_{pc}=\frac{m\sigma_Yth^2}{2\sin\alpha}$ and $M_{pf}=\sigma_YBt_fh$ are defined as the fully plastic bending moment of the

core and face sheets respectively.

M_Y in Eq.(11) and M_p in Eq.(12) have the following relationship,

$$\frac{M_p}{M_Y}=\frac{M_{pc}+M_{pf}}{\frac{2}{3}M_{pc}+M_{pf}} \tag{13}$$

For a monolithic plate with rectangular cross-section under bending load, the relationship between the fully plastic bending moment and the bending moment when the outermost layer starts to yield is $M_p=\frac{3}{2}M_Y$.

The expression of the initial collapse force F_0 is the same as that for the monolithic plate (see Appendix Eq.(A1)), $F_0=4M_p/L$, and it is compared with the peak force of the force-displacement curves under three-point bending (see Fig. 20). When the core wall is thick, i.e. t is large, the analytical results match well with that from the FEA, while when the core is thin, the peak force is much lower than the analytical results. It is because when the core is thin, it is prone to elastic buckling before the material reaches yielding. The peak force is governed by elastic buckling of the thin core under compression. After the initial buckling of the core, its load-carrying capacity reduces [19].

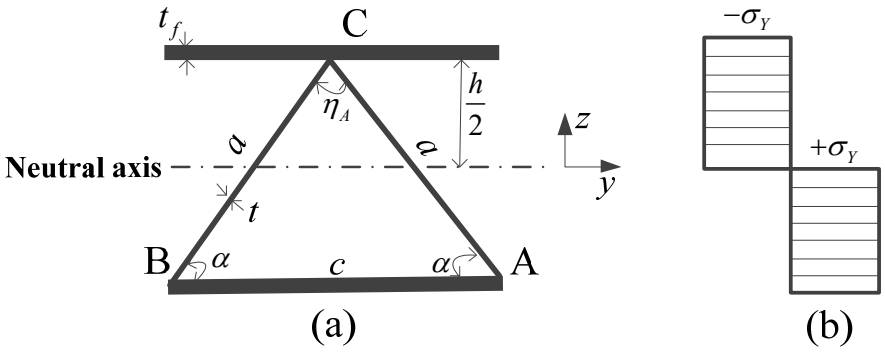

Fig. 19 Fully plastic bending moment: (a) sketch of cross-section of the sandwich plate; (b) stress distribution

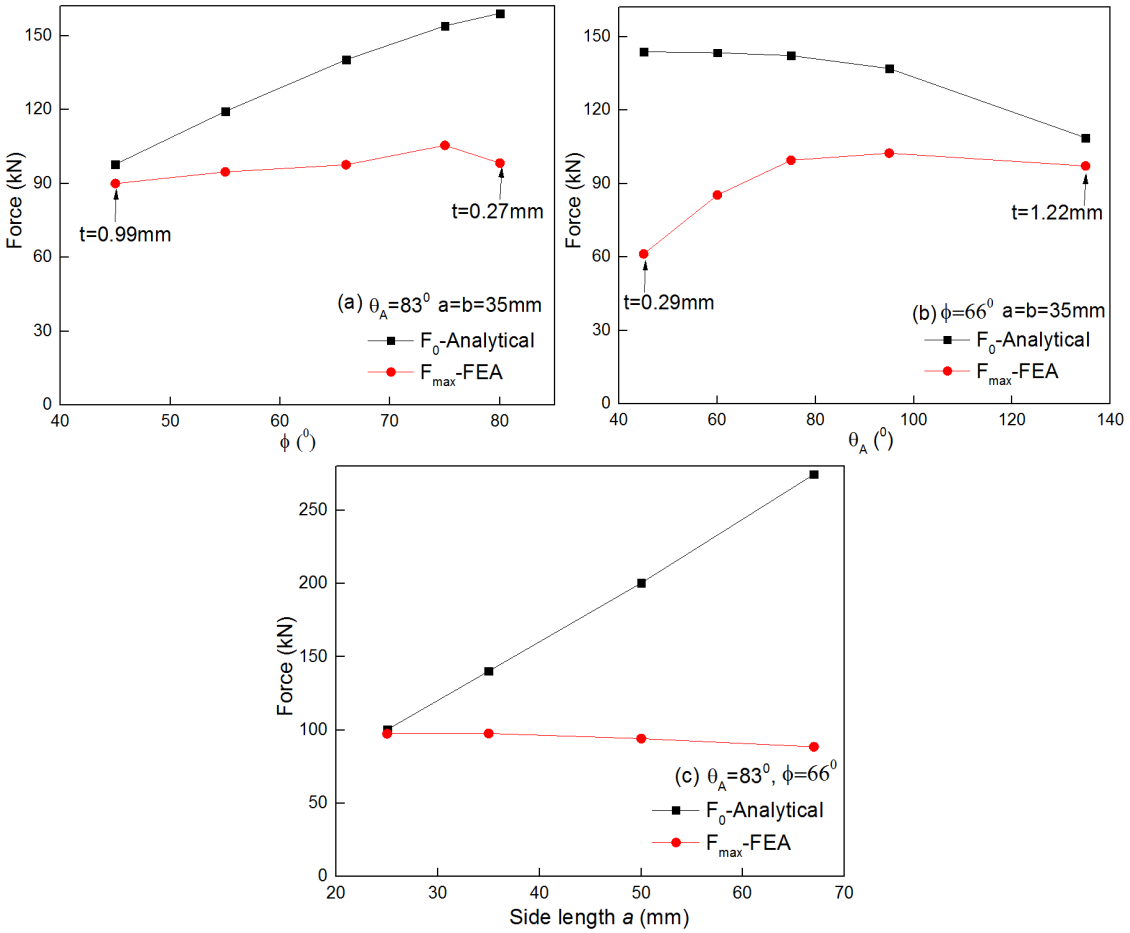

Fig. 20 Comparison of F_0 from theoretical analysis and $F_{\max}$ from FEA: (a) different values of ϕ; (b) different values of θ_A; (c) different values of side lengths

4.3 Elastic buckling moment, M_b

Fig. 21 shows the incipience of core buckling at the cross-section A-A of one cell. Fig. 21 (a) is for the core model with $\phi = 55^0$ and $\theta_A = 83^0$, and when the displacement is 7.2 *mm*, buckling is clearly observed. It is located at the plateau stage in the corresponding force-displacement curve (see Fig. 21 (c)). Fig. 21 (b) is for the core model with $\phi = 80^0$ and $\theta_A = 83^0$, and when the displacement is 3.6 *mm*, buckling is clearly observed. It is located at the peak in the corresponding force-displacement curve (see Fig. 21 (c)).

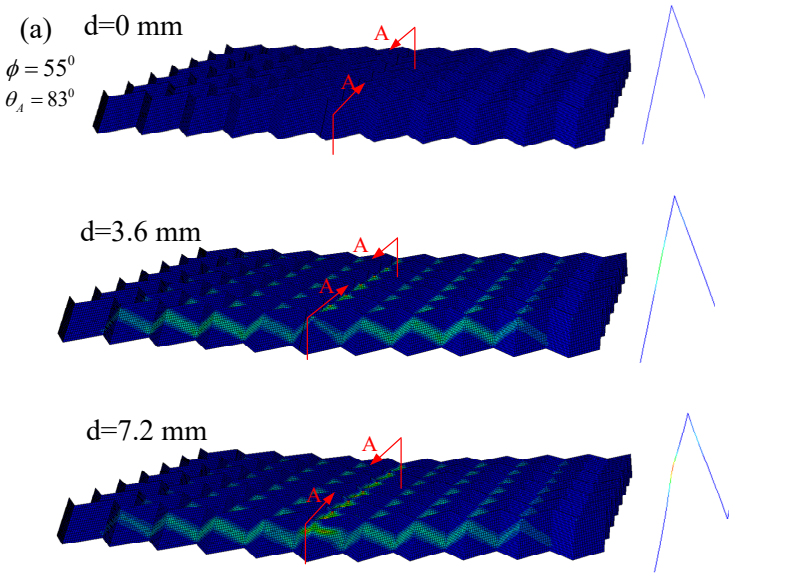
(a)
d=0 mm
$\phi = 55^0$
$\theta_A = 83^0$
A
A
d=3.6 mm
A
A
d=7.2 mm
A
A
Core model
Profile of one cell at
A-A cross-section

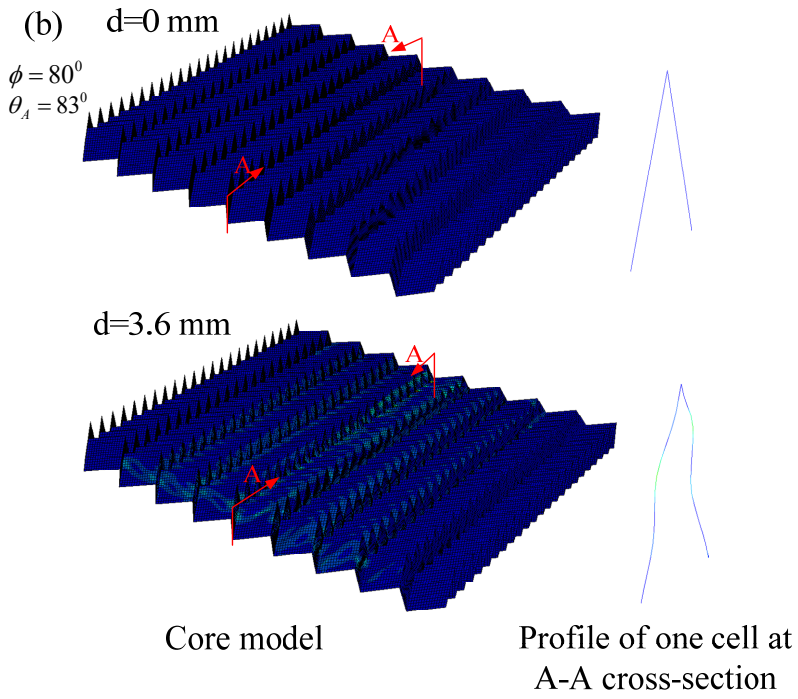
(b)
d=0 mm
$\phi = 80^0$
$\theta_A = 83^0$
A
A
d=3.6 mm
A
A
Core model
Profile of one cell at
A-A cross-section

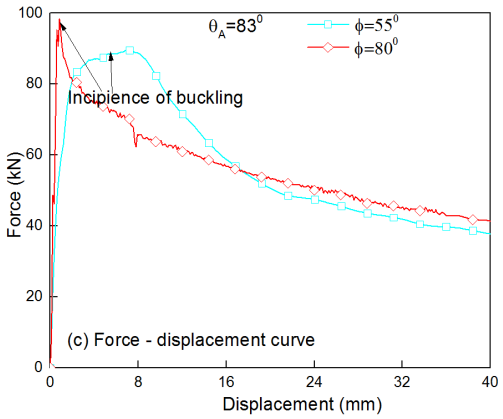

(c) Force-displacement curves

Fig. 21 Incipience of core buckling: (a) core model with $\phi = 55^0$ and $\theta_A = 83^0$; (b) core model with $\phi = 80^0$ and $\theta_A = 83^0$; (c) force-displacement curves

The maximum force ($F_{\max}$) in the force-displacement curves from FEA also represents the maximum bending strength, which is $M_{\max} = F_{\max} L / 4$. The buckling stress (σ_b) can be calculated from

$$\sigma_b = \frac{M_{\max} \cdot \frac{h}{2}}{I_y} \tag{14}$$

The calculated buckling stress is listed in Table 1 and it decreases with the increasing value of ϕ and side length, but increases as θ_A increases. Most of the buckling stresses are much lower than the yield stress of the core material (200 *MPa*), except for the specimens with the thickest core in Group 1 and 2 and the smallest cell in Group 3. Therefore, the maximum bending strength is mostly governed by elastic buckling of the core compression. The double logarithmic relationship between $\frac{\sigma_b}{E}$ and $\frac{t}{c}$ is shown in Fig. 22 and there is

$$\frac{\sigma_b}{E} = 0.044 \left(\frac{t}{c} \right)^{1.03} \tag{15}$$

where E is the young's modulus of the material.

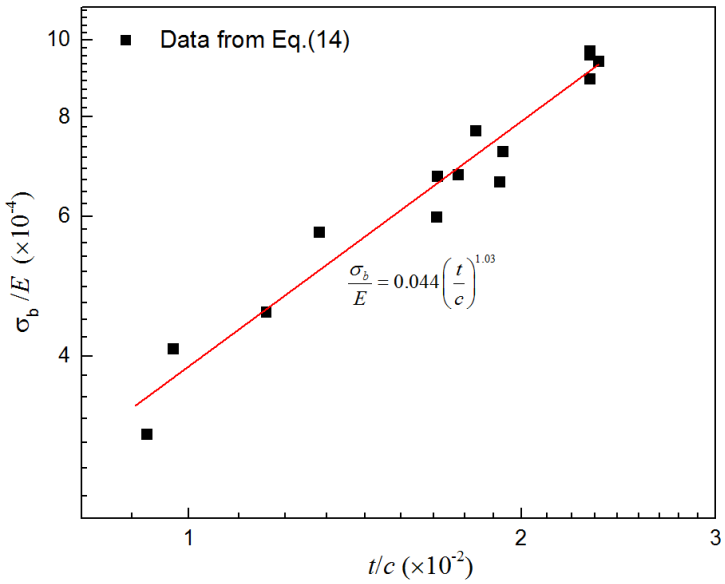

Fig. 22 The double logarithmic relationship between $\frac{\sigma_b}{E}$ and $\frac{t}{c}$

The empirical expression of the elastic buckling moment can be obtained from Eqs. (11) and (15) as follows,

$$\begin{aligned} M_b &= \sigma_b \left(\frac{mth^2}{3\sin\alpha} + Bt_f h \right) \\ &= 0.044E\left(\frac{t}{c}\right)^{1.03}\left(\frac{mth^2}{3\sin\alpha} + Bt_f h \right) \end{aligned} \tag{16}$$

5. Discussion

Several assumptions were adopted in the FEA and analytical study. Firstly, the material model without strain hardening was used in order to conduct analytical study and then compare the results between those from FEA and analytical work. In real applications, the strain hardening of the material should be considered. Secondly, it is an idealised condition that the core and the face plates were tied together, but there may be interfacial debonding under loadings in practice. Finally, the analytical study was simplified and only a few main parameters were used to characterize the mechanical properties of the sandwich structures with foldcore.

In this section, the response of a corresponding monolithic plate will be compared and the influences of the thickness of face sheets and the boundary conditions will be also discussed.

5.1 FEA of a monolithic plate

A monolithic plate with the same material property, mass and area as the sandwich plate was generated. The thickness of the plate was d=11.60 *mm*. The elements were solid element, type C3D8R, and the mesh size was 2 *mm*. FEA of the monolithic plate under three-point bending (see Fig. 23(a)) and static uniformly distributed pressure loading (see Fig. 23(b)) was conducted.

For three-point bending load, compressive force and energy absorption of the monolithic plate are much lower than the sandwich plates (see Fig. 11). The plateau force for the monolithic plate is around 37% of the maximum force for the sandwich plates. Final force of the sandwich structures approaches to the plateau force of the monolithic plate (see Fig. 11). Energy absorbed by the monolithic plate is around half of the sandwich plates (see Fig. 12).

For uniformly distributed pressure loading, when pressure is small, deformation of the monolithic plate is larger than or the same as that of the sandwich plates (see Fig. 15), and energy absorption capacity is almost the same for the two structures (see Fig. 17). When pressure is large, the monolithic plate deforms less than sandwich plates (see Fig. 15), but the energy absorption capacity for sandwich plates is larger than the monolithic plate (see Fig. 17). This result is similar to the comparison of sandwich beams and the corresponding monolithic beams under blast loading in Ref. [18].

The initial collapse force of a monolithic plate under three-point bending and the relationship between the pressure and displacement under static uniformly distributed pressure are employed in Appendix A.1 and A.2 respectively. The comparison of FEA and analytical results are presented in Fig. A1 and A3.

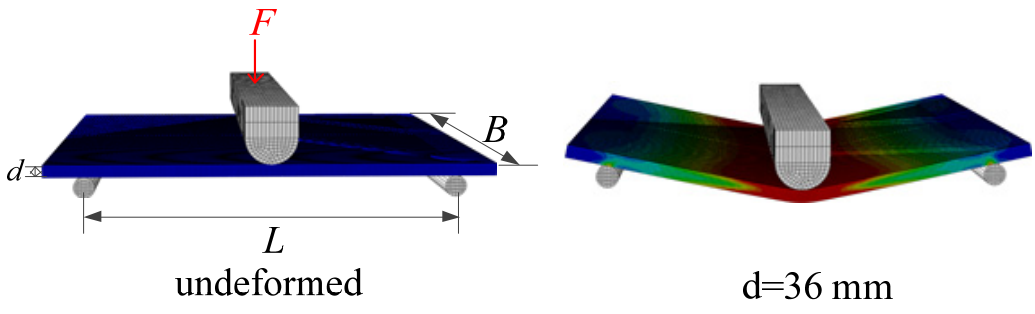

(a) quasi-static three-point bending

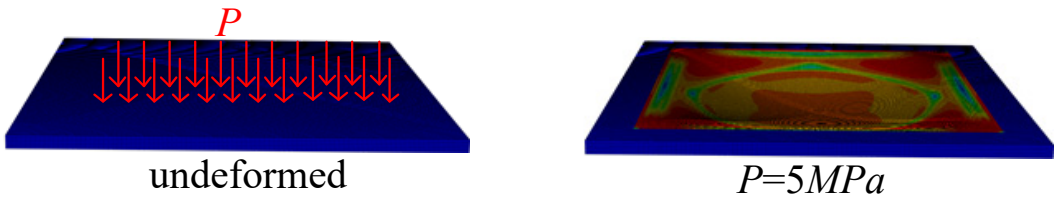

(b) static uniformly distributed pressure

Fig. 23 FEA of a monolithic plate: (a) quasi-static three-point bending; (b) static uniformly distributed pressure (the plot contours denote the Mises Stress)

5.2 Influence of thickness of the face sheet

Four different thicknesses of the face sheet were investigated, which were 2 *mm*, 3 *mm*, 4 *mm* and 5 *mm* respectively. The parameters for the core were $\phi = 66^0$, $\theta_A = 135^0$ and side lengths *a*=*b*=35 *mm*. The force-displacement curves are shown in Fig. 24(a). For this kind of Miura-ori core, the calculated buckling stress is 187.8 *MPa* (shown in Table 1), which is smaller than the yield stress of the core material (200 *MPa*). Therefore, the peak force is governed by the core buckling and the elastic buckling moment can be obtained from Eq.(16), then the initial collapse force F_0 can be calculated. The maximum force from FEA is plotted as the square scatters in Fig. 24(b). The circle scatters denote the analytical results of the initial collapse force F_0 and they match well with the results from FEA.

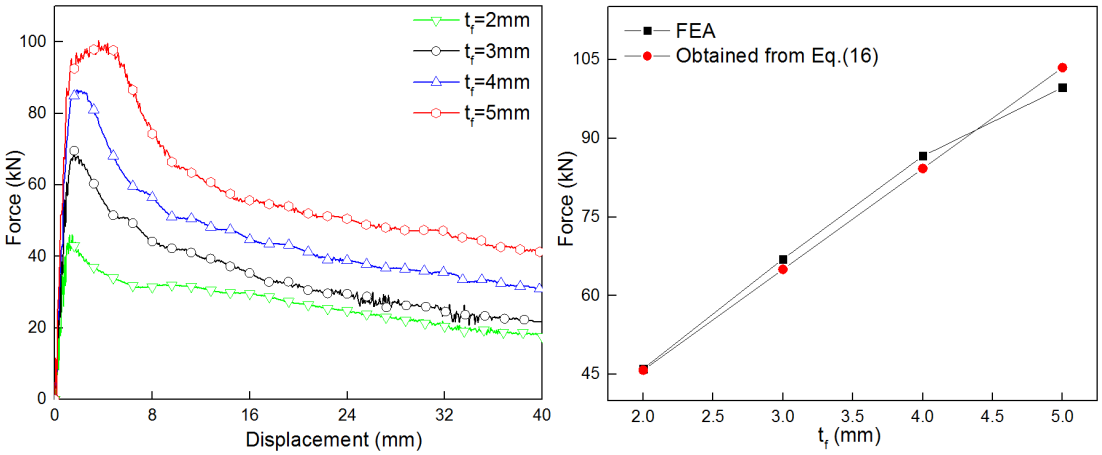

(a) force-displacement curves (b) comparison of FEA and analytical results

Fig. 24 Influence of thickness of the face sheet: (a) force-displacement curves; (b) comparison of FEA and analytical results

5.3 Influence of the boundary condition

Effect of boundary conditions was investigated. FEA models are shown in Fig. 25(a). The parameters for the core were $\phi = 66^0$, $\theta_A = 95^0$ and side lengths a=b=35 mm. For the clamped boundary, two sides of the sandwich plates were clamped and two supporters in three-point bending loading condition were removed. Force-displacement curves are compared for the two boundary conditions in Fig. 25(b). In the elastic deformation stage, the two curves are almost the same. However, when the plastic deformation takes place, the force for the simply supported boundary condition is at a plateau stage. Then the sandwich plate undergoes subsequent softening due to buckling within the core and its load-carrying capacity reduces. For the clamped boundary condition, force continues to increase dramatically after the elastic deformation due to the increasing stretching force at the two clamped sides. Fig. 25(c) shows the displacement of the mid-span of the top and bottom face sheets for the two boundary conditions. The horizontal axis is the displacement of the indenter, which is the same as the displacement at the mid-span of the top face sheet, and the vertical axis is the displacement at the mid-span of the bottom face sheet. It shows that at the early deformation stage, the sandwich plate deforms as a whole, and then the core is compressed for both of the boundary conditions. The core compression is almost the same for the two boundary conditions.

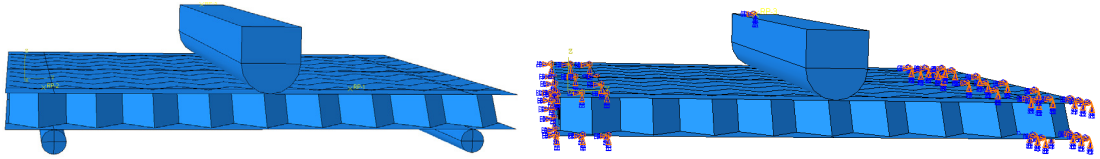

Simply supported Clamped

(a) FEA models

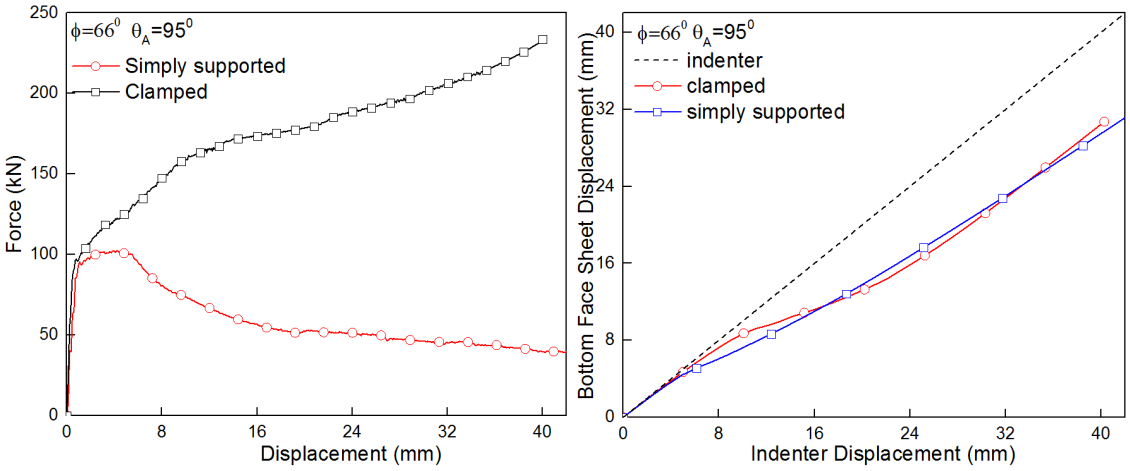

(b) force-displacement curves (c) displacement at the mid-span of the bottom face sheet

Fig. 25 Influence of the boundary condition: (a) FEA models; (b) force-displacement curves; (c) displacement of the indenter and the mid-span of the bottom face sheet

PLASTIC DEFORMATION MECHANISMS IN AXIALLY

6. Conclusions

A parametric study of sandwich plates with Miura-ori core was investigated by means of FEA. The sector angle (ϕ), lateral dihedral angle (θ_A) and side lengths (a and b) were set as variable values of the Miura-ori core for parametric study. Two cases of loadings were studied: quasi-static three-point bending and static uniformly distributed pressure loading. The load-displacement curves were obtained and energy absorption performance was assessed. Theoretical analysis of monolithic and sandwich plates was conducted and the analytical results match well with FEA result. Some conclusions are obtained, as follows.

(1) Three-point bending: For different sector angles (ϕ), when $\phi = 55^0$ and $\phi = 66^0$, sandwich

plates have the best energy absorption capacity, but the one with $\phi = 55^0$ has slightly lower peak force and longer plateau of the compressive force. For different lateral dihedral angles (θ_A), when $\theta_A = 95^0$, sandwich plate has the best energy absorption capacity and the highest peak force. For different side lengths, the peak force is almost the same. Softening due to core buckling is prone to taking place as the side lengths increase. Energy absorption capacity decreases as the side lengths increase. A corresponding monolithic plate was also investigated by using FEA and it is found that all the sandwich plates perform better. Energy absorbed by the monolithic plate is around half of the sandwich plates.

(2) Static uniformly distributed pressure loading: The core compression increases with the increasing sector angle (ϕ) and side length (a and b). When pressure is small, deformation of the monolithic plate is larger than or the same as the sandwich plates, and the energy absorption capacity is almost the same for the two structures. When pressure is large, monolithic plate deform less than the sandwich plates, and energy absorption capacity for the sandwich plates is larger than the monolithic plate.

(3) For the sandwich plate, the maximum bending strength is governed by the incipience or fully plastic yielding of the core material for relatively thick cores, or elastic buckling of the core compression for thin cores. After initial buckling of the core, its load-carrying capacity reduces. The yielding moment, fully plastic bending moment and elastic buckling moment of the incipience of core buckling were analysed.

Acknowledgements

The authors thank the support by the National Natural Science Foundation of China under grant number 51578361, the National Key Research and Development Plan under grant number 2016YFC0701100, and the Tianjin Basic Research Program under grant number 15JCZDJC39900. The authors, XM Xiang and G Lu, also thank the Australian Research Council for the financial support through a Discovery Grant (DP160102612).

Appendix

Theoretical analysis of a monolithic plate

A.1 Three-point bending

For three-point bending load, the initial collapse force is found to be [19]

$$F_0 = 4M_p / L \tag{A1}$$

where $M_p = \dfrac{\sigma_y B d^2}{4}$ is the fully plastic bending moment, σ_y is the yield stress, B is the width, d is the thickness and L is the support span. When the width is much larger than the thickness of the plate, σ_y is taken as multiplied $2/\sqrt{3}$ by the yield stress in simple tension in order to account for the plane strain condition [19]. Therefore, the initial collapse force for the monolithic plate in this research work is

$$F_0 = \frac{2\sigma_y B d^2}{\sqrt{3}L} \tag{A2}$$

The comparison of analytical and FEA results is shown in Fig. A1and they match well.

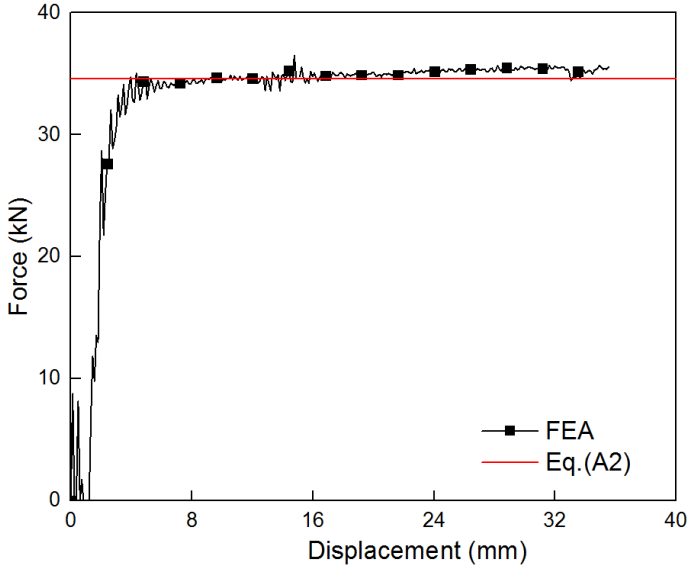

Fig. A1 Comparison of analytical and FEA results

A.2 Static uniformly distributed pressure

For a rectangular plate under static uniformly distributed pressure loading, the upper bound (p^u) and lower bound (p^l) of the initial static collapse pressure were given by Jones [20],

$$p^u = 12M_p \Big/ \left[\left(\frac{B}{2} \right)^2 \left(\sqrt{3+\beta^2} - \beta \right)^2 \right] \tag{A3}$$

$$p^l = 4M_p \left(1+\beta^2\right) \Big/ \left(\frac{B}{2} \right)^2 \tag{A4}$$

where $\beta = B / L$.

The deformation profile of a fully clamped monolithic plate under uniformly distributed pressure is shown in Fig. A2. The plate is divided into four rigid zones by the plastic hinges (see Fig. A2(a)) and the plastic flows are distributed in the plastic hinges. The relationship between pressure (p) and the final displacement displacement (W) is given by Jones [20],

$$p / p_c = \begin{cases} 1 + \dfrac{\left[\xi_0 + \left(3 - 2\xi_0\right)^2 \right] \left(W/d\right)^2}{3\left(3-\xi_0\right)} & W/d \le 1 \\ \left(2W/d\right)\left[1 + \xi_0\left(2-\xi_0\right)\left(d^2/3W^2 - 1\right)/\left(3-\xi_0\right)\right] & W/d > 1 \end{cases} \tag{A5}$$

where p_c is the initial static collapse pressure, $\xi_0 = \beta \tan\varphi$ and $\tan\varphi = -\beta + \sqrt{3+\beta^2}$. When p_c is set as the lower bound of the initial static collapse pressure (p^l) in Eq. (A4), the relationship between the dimensionless pressure (p / p_c) and dimensionless displacement (W / d) is shown in Fig. A3 and the analytical result matches well with FEA result.

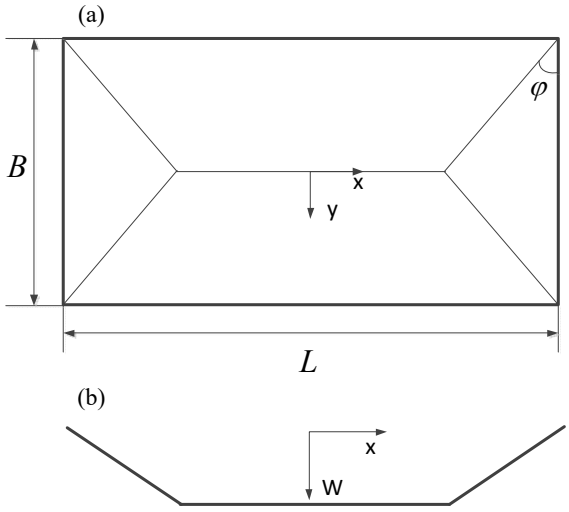

Fig. A2 Deformation profile of a fully clamped monolithic plate under uniformly distributed pressure: (a) top view; (b) front view

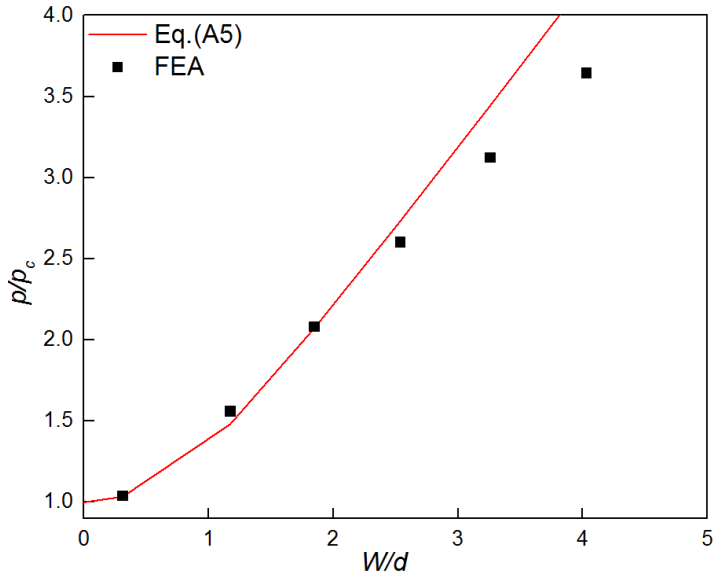

Fig. A3 Comparison of analytical and FEA results

References

[1] Gattas JM, You Z. Quasi-static impact of indented foldcores. International Journal of Impact Engineering. 2014;73:15-29.

[2] Kintscher M, Kärger L, Wetzel A, Hartung D. Stiffness and failure behaviour of folded sandwich cores under combined transverse shear and compression. Composites Part A: Applied Science and Manufacturing. 2007;38:1288-95.

[3] Li T, Wang L. Bending behavior of sandwich composite structures with tunable 3D-printed core materials. Composite Structures. 2017;175:46-57.
[4] Tachi T. Freeform rigid-foldable structure using bidirectionally flat-foldable planar quadrilateral mesh. Advances in Architectural Geometry. 2010:87-102.
[5] Thrall A, Quaglia C. Accordion shelters: a historical review of origami-like deployable shelters developed by the US military. Engineering Structures. 2014;59:686-92.
[6] Fischer S, Drechsler K, Kilchert S, Johnson A. Mechanical tests for foldcore base material properties. Composites Part A: Applied Science and Manufacturing. 2009;40:1941-52.
[7] Gattas JM, You Z. The behaviour of curved-crease foldcores under low-velocity impact loads. International Journal of Solids and Structures. 2015;53:80-91.
[8] Liu S, Lu G, Chen Y, Leong YW. Deformation of the Miura-Ori Patterned Sheet. International Journal of Mechanical Sciences. 2015.
[9] Zhou X, Wang H, You Z. Mechanical properties of Miura-based folded cores under quasi-static loads. Thin-Walled Structures. 2014;82:296-310.
[10] Gattas JM. Quasi-static impact of foldcore sandwich panels: University of Oxford; 2013.
[11] Yang K, Xu S, Shen J, Zhou S, Xie YM. Energy absorption of thin-walled tubes with pre-folded origami patterns: Numerical simulation and experimental verification. Thin-Walled Structures. 2016;103:33-44.
[12] Zang S, Zhou X, Wang H, You Z. Foldcores made of thermoplastic materials: Experimental study and finite element analysis. Thin-Walled Structures. 2016;100:170-9.
[13] Fischer S. Aluminium foldcores for sandwich structure application: Mechanical properties and FE-simulation. Thin-Walled Structures. 2015;90:31-41.
[14] Heimbs S, Cichosz J, Klaus M, Kilchert S, Johnson AF. Sandwich structures with textile-reinforced composite foldcores under impact loads. Composite Structures. 2010;92:1485-97.
[15] Pydah A, Batra RC. Crush dynamics and transient deformations of elastic-plastic Miura-ori core sandwich plates. Thin-Walled Structures. 2017;115:311-22.
[16] Heimbs S. Virtual testing of sandwich core structures using dynamic finite element simulations. Computational Materials Science. 2009;45:205-16.
[17] Schenk M, Guest SD, McShane GJ. Novel stacked folded cores for blast-resistant sandwich beams. International Journal of Solids and Structures. 2014;51:4196-214.
[18] Xiang XM, Lu G, Ma GW, Li XY, Shu DW. Blast response of sandwich beams with thin-walled tubes as core. Engineering Structures. 2016;127:40-8.
[19] Lu G, Yu TX. Energy absorption of structures and materials. Cambridge: Woodhead Publishing; 2003.
[20] Jones N. Structural Impact. Cambridge: Cambridge University Press; 1989.